DEPARTMENT OF DEFENCE
DEFENCE SCIENCE & TECHNOLOGY ORGANISATION
DSTO

Development of Film-Infused Tougher Boron/Epoxy Ply

Peter Chalkley, Ivan Stoyanovski,
Richard Muscat and Andrew Rider

DSTO-TN-0308

Development of Film-Infused Tougher Boron/Epoxy Ply

Peter Chalkley, Ivan Stoyanovski, Richard Muscat and Andrew Rider

Airframes and Engines Division
Aeronautical and Maritime Research Laboratory

DSTO-TN-0308

ABSTRACT

A previous study has examined the fatigue properties of bonded joints representative of the boron-epoxy doublers bonded to the wing-pivot fittings of Royal Australian Air Force (RAAF) F-111C aircraft. These repairs indicated some fatigue damage and crack propagation occurred at the boron fiber to adhesive interface of the doubler. This paper reports studies that have investigated methods to improve the fracture toughness of the boron/epoxy laminate. Two types of specimen were prepared. In the first case the standard boron epoxy laminate was modified by co-curing FM73 adhesive film layers at the midplane. In the second case a standard laminate with two FM73 film infused layers at the midplane was prepared. The two modified laminates showed substantial increases in the fracture toughness, however, the co-cured FM73 laminate did not exhibit stable fracture. Failure analysis indicated that the three laminate specimens tested exhibited a complex fracture. Fracture either propagated at the boron-epoxy interface or within the resin or FM73 layers. Further improvement in fracture toughness of the laminate may be achieved by improving the boron to FM73 adhesion. The methods reported for improving laminate fracture toughness may potentially be employed for aircraft repairs in which very high stresses are known to be present.

Published by

DSTO Aeronautical and Maritime Research Laboratory
PO Box 4331
Melbourne Victoria 3001 Australia

Telephone: (03) 9626 7000
Fax: (03) 9626 7999

AR-011-599
October 2000

APPROVED FOR PUBLIC RELEASE

Development of Film-Infused Tougher Boron/Epoxy Ply

Executive Summary

A previous study has examined the fatigue properties of bonded joints representative of the boron-epoxy doublers bonded to the wing-pivot fittings of Royal Australian Air Force (RAAF) F-111C aircraft. These repairs indicated some fatigue damage and crack propagation occurred at the boron fiber to adhesive interface of the doubler. This paper reports studies that have investigated methods to improve the fracture toughness of the boron/epoxy laminate. Two types of specimen were prepared. In the first case the standard boron epoxy laminate was modified by co-curing FM73 adhesive film layers at the midplane. In the second case a standard laminate with two FM73 film infused layers at the midplane was prepared. The two modified laminates showed substantial increases in the fracture toughness, however, the co-cured FM73 laminate did not exhibit stable fracture. Failure analysis indicated that the three laminate specimens tested exhibited a complex fracture. Fracture either propagated at the boron-epoxy interface or within the resin or FM73 layers. Further improvement in fracture toughness of the laminate may be achieved by improving the boron to FM73 adhesion. The methods reported for improving laminate fracture toughness may potentially be employed for aircraft repairs in which very high stresses are known to be present.

Contents

1. Introduction

A previous study has examined the fatigue properties of bonded joints representative of the boron-epoxy doublers bonded to the upper plate splice region of the wing-pivot-fittings of Royal Australian Air Force (RAAF) F-111C aircraft [1]. These studies indicated that the original doublers were designed with a low margin of safety in fatigue, especially when exposed to moisture and aged fuel. Fatigue damage and crack propagation in the representative bonded joints indicated that failure occurred either at the aluminium to adhesive interface or at the boron to adhesive interface [Figure 1.1]. Stress analysis performed on the bonded joint showed that one of the factors contributing to the lower fatigue tolerance was the relatively high angle of effective taper of the doublers. Current repairs would have employed a much lower taper angle and, therefore, provided improved fatigue tolerance. Additional means of increasing the fatigue tolerance of the bonded joints would also be to improve the fracture toughness of the boron-adhesive interface.

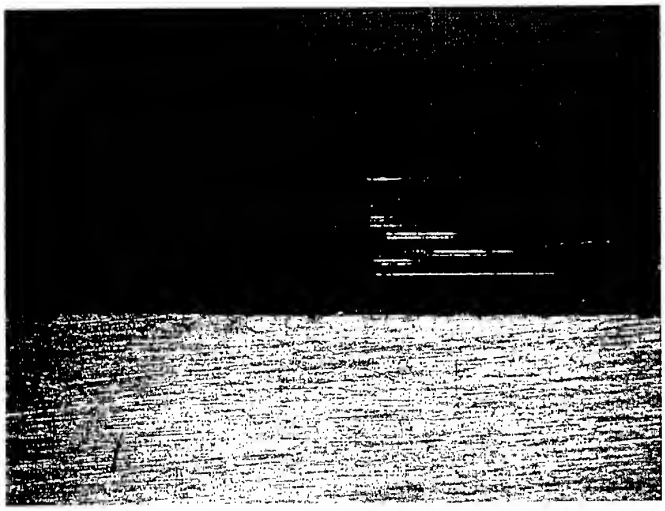

Figure 1.1. *Fatigue crack propagation in a skin doubler specimen. Details of this specimen are provided in [1].*

Scanning electron microscopy (SEM) examination of the skin doubler regions, where adhesive to boron failure occurred, revealed that the fatigue crack propagated within the boron-epoxy ply adjacent to the adhesive in the resin rich area between the boron fibres and the adhesive-resin interface [Figure 1.2 and 1.3].

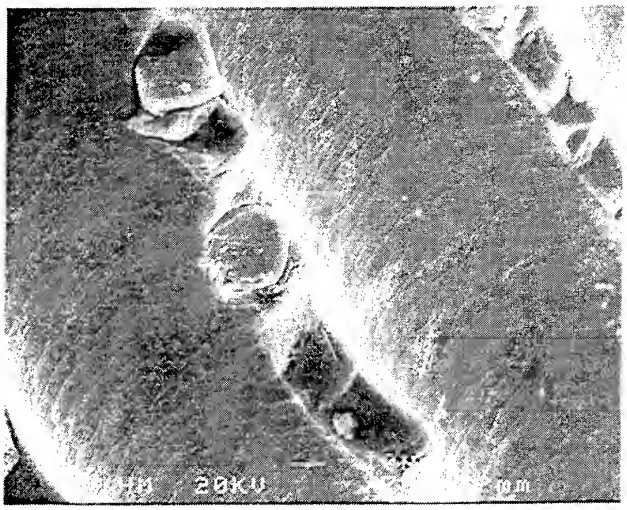

Figure 1.2. *Fatigue failure surface – adhesive side showing the hollow impression in the resin from the boron fibres.*

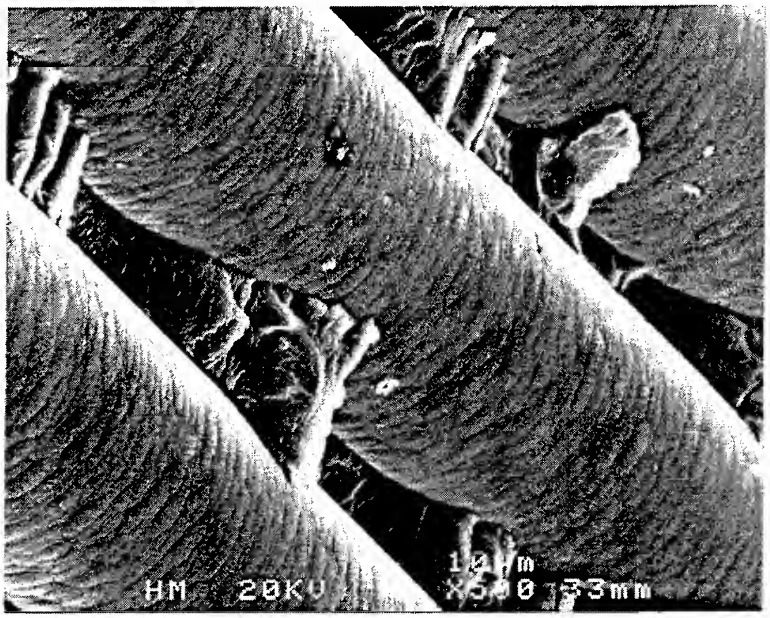

Figure 1.3. *Fatigue failure surface – boron/epoxy laminate side. The image shows the boron fibres and the regions of cohesive resin failure in between the fibres.*

Figures 1.2 and 1.3 show that the fatigue failure is occurring in two places in the 5521/4 lamina:

1. At the interface between the boron fibres and the resin
2. Within the resin in the valleys between the fibres.

Clearly, the toughness of this system could be improved by increasing the toughness of the resin and/or by increasing the interfacial bond strength between the fibres and the resin. This report investigates the use of film infusion of FM73 adhesive into dry boron fibres to create a tougher boron/matrix ply. The test method ASTM 5528-94a , Mode I Interlaminar Fracture toughness of Unidirectional Fiber-Reinforced Polymer Matrix Composites, was used to investigate toughness changes [2].

2. Manufacture of FM73 Infused Boron Lamina

Materials used in making a layer of FM73 film infused boron were:

1. Boron Woven Fabric (part no. 260-100046-001). This is unidirectional 0.004 inch diameter fibres with a light polyester weave to maintain the fibres in a closely woven mat.
2. Cytec FM73 with a density of 0.085 psf . This is the adhesive used in standard repairs and contains a polyester knit carrier for bondline thickness control and handling.

The layer was made by sandwiching the fibres and adhesive between two layers of teflon coated glass and applying pressure and a temperature of 80°C for 20 minutes (see Fig. 2.1). The finished product is shown in Fig. 2.2.

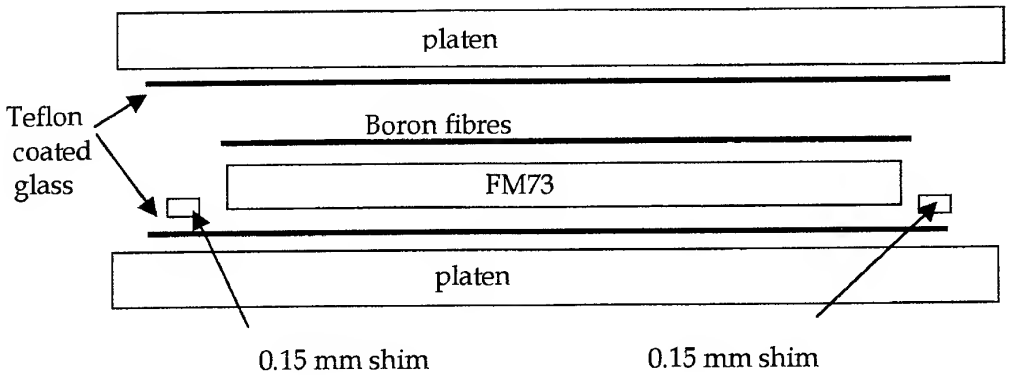

Figure 2.1. Schematic of the assembly for the film infused boron.

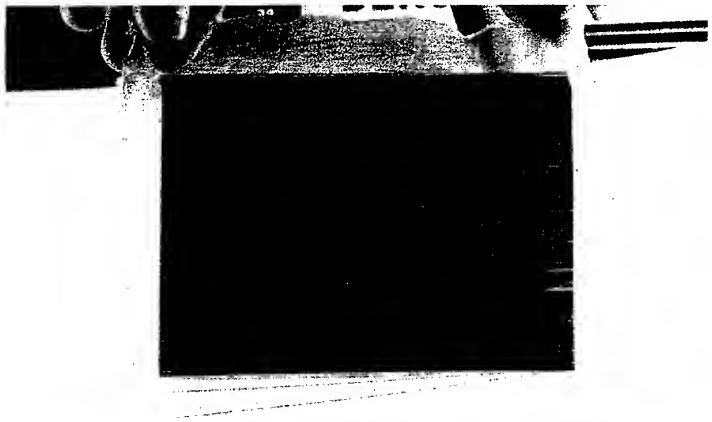

Figure 2.2 A layer of FM73 film infused boron.

3. Specimen Manufacture

Three panels of sixteen plies of unidirectional boron/matrix lamina were made:

1. A standard laminate made entirely of 5521/4 lamina.
2. A laminate made of sixteen 5521/4 lamina co-cured with two layers of FM73 at the centre.
3. A laminate made of fourteen 5521/4 lamina co-cured with two laminae of dry boron fibres infused with FM73.

The last two laminates can be considered to be functionally gradient laminates in that the manufacturer's standard plies are swapped for tougher plies at the location where maximum toughness is needed – adjacent to the bondline.

Each panel was 160 mm by 150 mm by 16 plies. A strip of Teflon (0.025 mm thickness) 60 mm by 150 mm was placed at the centre of the laminate to provide the starter crack. The panels were cut into six specimens of 20 mm x 160 mm with piano hinges applied using 5 minute Araldite. Figures 3.1, 3.2 and 3.3 show schematics of each panel. The panels were cured in an autoclave. Each panel was cured for 1 hour at 120°C with a heating ramp of 5°C/minute and 300 kPa pressure. The autoclave cure arrangement was as shown in Figure 2.1.

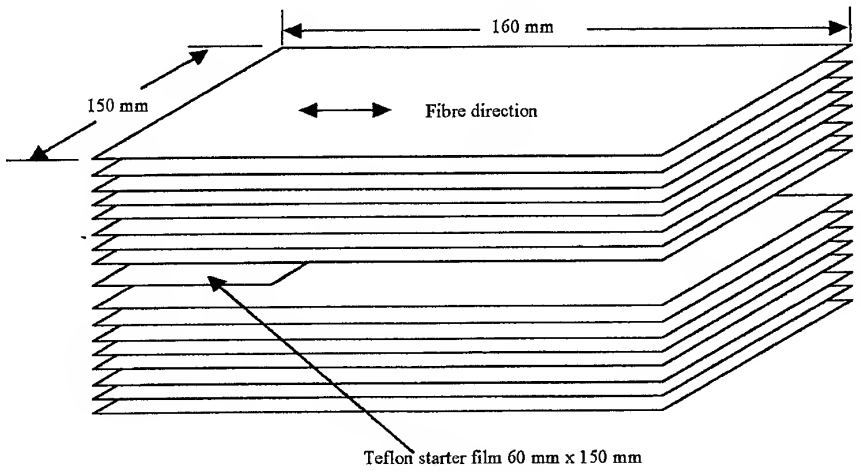

Figure 3.1. Standard 16 plies 5521/4 panel with teflon crack starter.

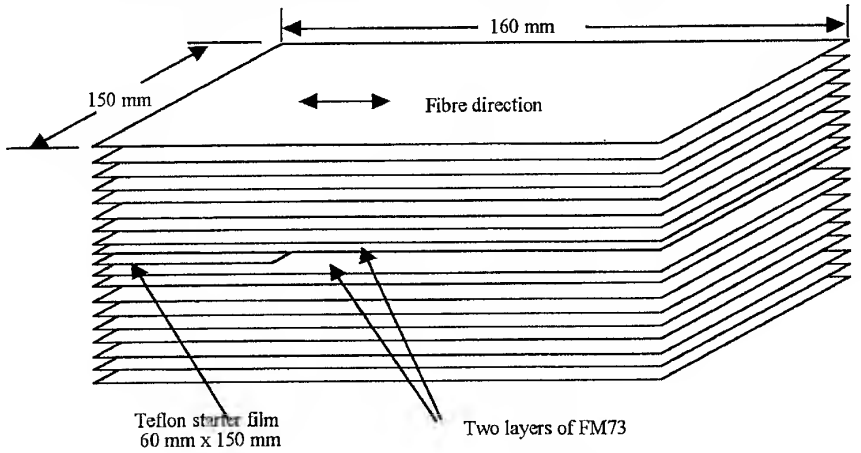

Figure 3.2. 16 plies 5521/4 laminate co-cured with two layers of FM73

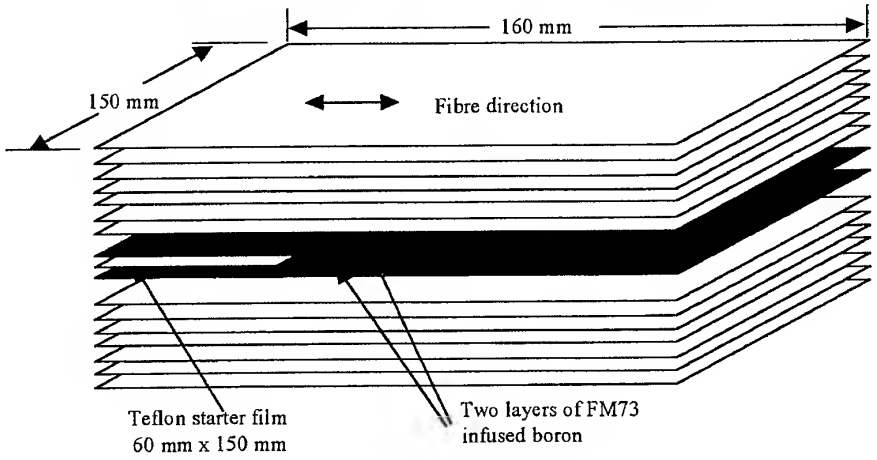

Figure 3.3. 14 plies 5521/4 plus two plies of FM73-infused boron.

4. Experimental

The test technique adhered to the technique prescribed in ASTM D5528-94a [2]. An 1121 Instron (10 kN capacity) was used with a 5 kN load cell. Load and crosshead displacement data was recorded on the machine's chart recorder. A scale was marked on the specimens ahead of the tip of the teflon implant as recommended in ASTM 5528-94a [1]. The scale marked was at approximately 1, 2, 3, 4, 5, 10, 15, 20 and 25 mm. Water based liquid paper was applied ahead of the tip and these positions marked using a fine ball point pen. Accurate measurements of the location of these marks and of distance of the tip of teflon implant from the hinge of the piano hinges was made using a travelling microscope. A crosshead rate of 0.5 mm/minute was applied and the load/displacement point at which the crack passed each scale position (as observed through the travelling microscope) was marked on the chart.

Two methods were used to determine the interlaminar fracture toughness, G_I; the Modified Beam Theory (MBT) method and the Compliance Calibration (CC) method. Values calculated using these theories are provided in the Appendix.

The MBT method used equation 1:

$$G_I = \frac{3P\delta}{2b(a+|\Delta|)} \qquad (1)$$

where P is the load recorded for the load point displacement, δ, with delamination length, a, and specimen width, b. Correction for adherend rotation during loading is provided by the $|\Delta|$ term. This was determined by generating a least squares plot of the cube root of compliance, $C^{1/3}$, as a function of delamination length. The delamination length for zero compliance from the plot is the correction factor. The compliance is determined from δ/P for the measurements provided in the appendix.

The CC method used equation 2:

$$G_I = \frac{nP\delta}{2ba} \qquad (2)$$

where n is determined from the gradient of the log-log plot of δ/P versus a.

The fracture surfaces were analysed using X-ray Photoelectron Spectroscopy (XPS) and Scanning Electron Microscopy (SEM). XPS was performed by irradiating samples with a 150W AlK_α flux in a vacuum of $5x10^{-9}$ torr. Photoelectrons were analysed with a Fixed Retard Ratio of 24 and binding energy was referenced to the adventitious C 1s line at 285eV. Quantification used sensitivity factors provided by the manufacturer. SEM was performed with a 20kV electron beam on samples coated with a 0.5 μm layer of sputtered gold. XPS spectra of the boron fibre surface were also recorded as a function of depth with the use of an argon ion gun. Argon ions directed at the surface with 5kV potential eroded or etched the surface material at a rate of approximately 2nm/min. XPS spectra recorded during the etching gave a depth profile concentration of the elemental species in the surface layers of the fibre. XPS analysis provided

chemical information emanating from the first 5nm of the fracture surface and SEM micrographs provided visual details of the fracture process.

Optical images of the fracture surfaces were also recorded using a Leica MZ 12 optical microscope interfaced to a personal computer using Adobe Photoshop image capture and processing software.

5. Test Results

Dimensions and test results for each specimen are given in Appendix A. Figures 5.1, 5.2 and 5.3 show typical resistance curve plots (G_I versus a) for the three specimen types.

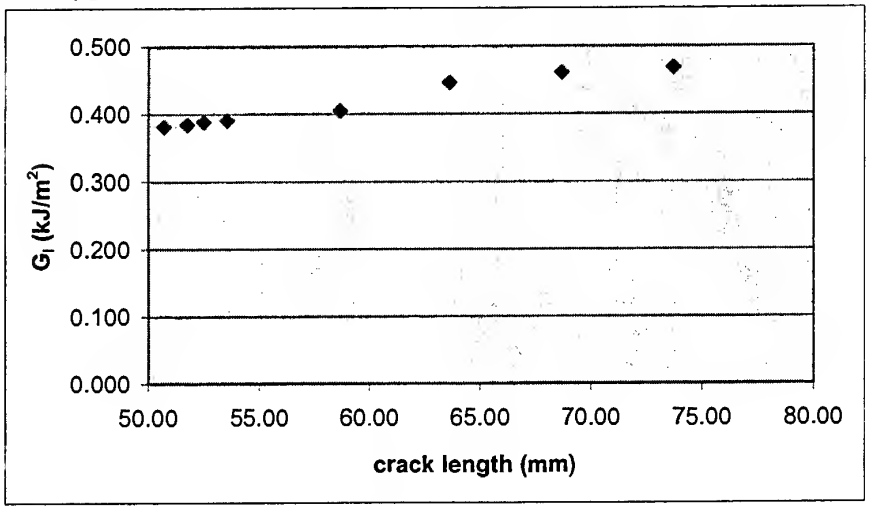

Figure 5.1. 5521/4 - resistance curve plot.

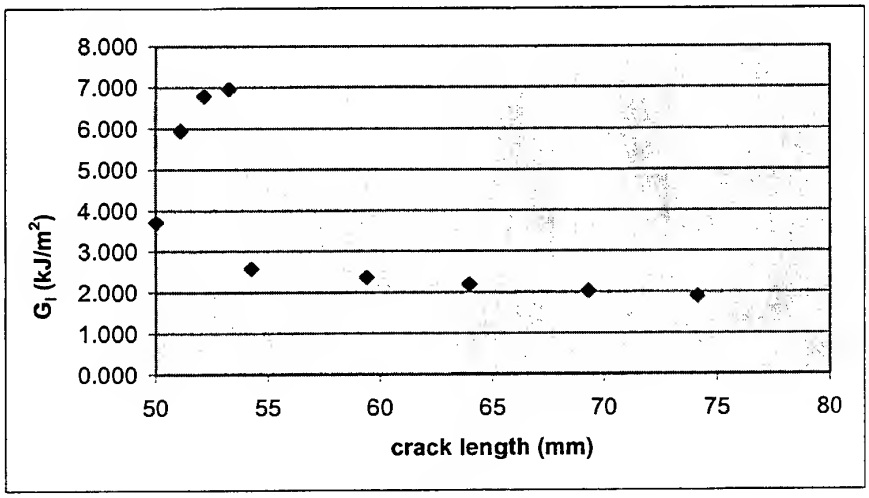

Figure 5.2. 16 plies 5521/4 co-cured with 2 layers FM73 - resistance curve plot.

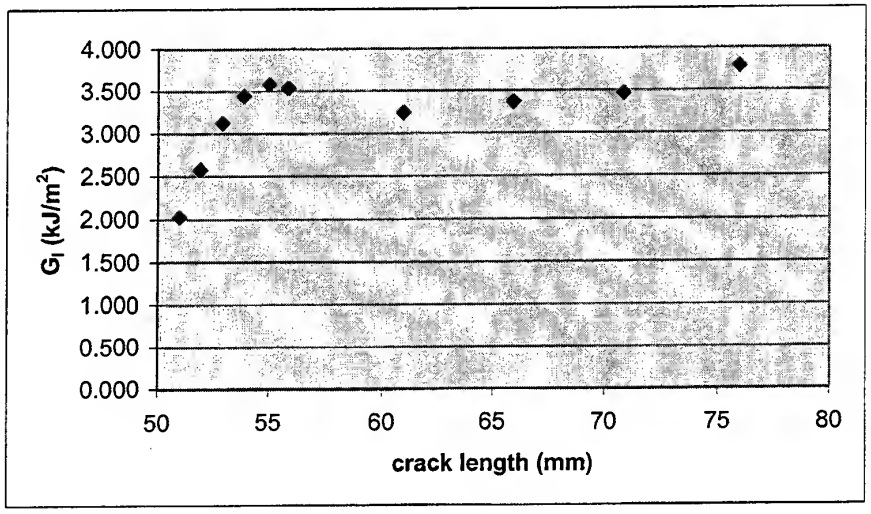

Figure 5.3. *14 plies 5521/4 co-cured with 2 plies FM73-infused boron - resistance curve plot.*

The initiation values of toughness are presented in Table 5.1.

Table 5.1. *Initiation fracture toughness values for the three laminate types.*

	5521/4	5521/4 + FM73	5521/4+infused boron
G_I (J/m²)	328	3109	1633
No specimens	4	6	6
Stand dev	41	612	280

Note that although the laminate with two layers of co-cured FM73 had a high initial toughness it was an essentially unstable fracture because the strain energy release rate decreased with increasing crack length after about 5 mm of crack growth. Indeed one specimen failed catastrophically after a small amount of crack growth [Figure 5.4].

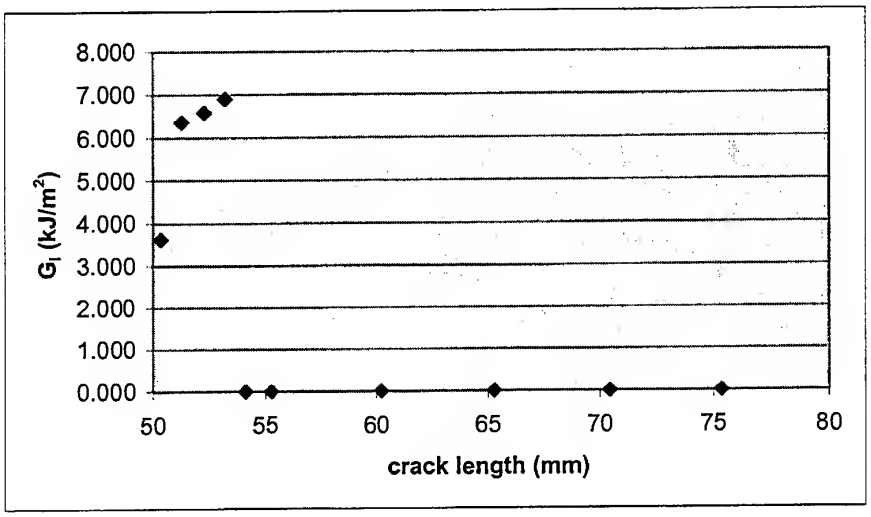

Figure 5.4. *14 plies 5521/4 co-cured with 2 plies FM73-infused boron – showing catastrophic failure at crack length of about 5 mm.*

All specimens showed some fibre bridging during testing. Only in the 5521/4 specimens did a single crack travel along the midplane. For the other specimens – the specimens with co-cured FM73 layers and the specimens with co-cured film infused boron layers - substantial secondary cracks appeared in addition to the primary crack. Neither the primary nor the secondary cracks were located at the midplane probably because this is a FM73 rich zone where the toughness could be expected to be the highest.

If more plies of FM73 film infused boron were added to that series of specimens then higher toughness values again could be expected. Cracking tended to occur in the standard 5521/4 plies either side of the toughened film infused plies.

Figures 5.5 and 5.6 show the test setup and a macro of the failure of a co-cured FM73 specimen.

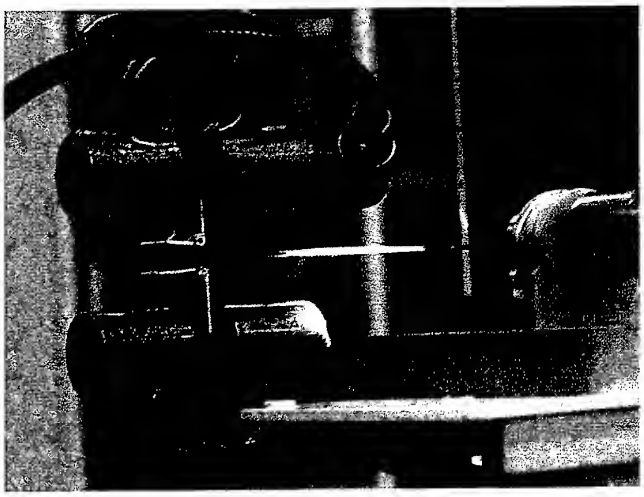

Figure 5.5. *Experimental arrangement used to determine the interlaminar fracture toughness G_I.*

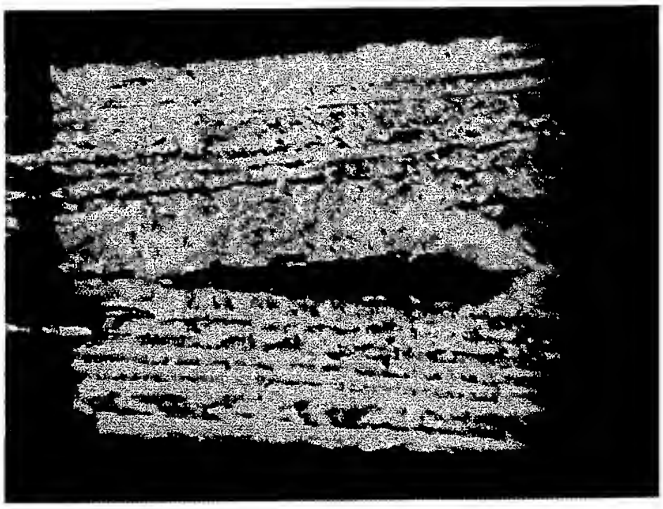

Figure 5.6. *Digital photographic image of the FM73 co-cured specimen showing fibre bridging.*

6. Fracture Analysis

Optical and SEM analysis of the failure surfaces tested in section 5 was undertaken to determine the fracture propagation modes. Alterations in the locus of fracture should

provide some indication of the mechanisms responsible for increasing the fracture toughness of the samples manufactured using the FM73 adhesive.

6.1 Optical Analysis of Standard 5521/4 laminate

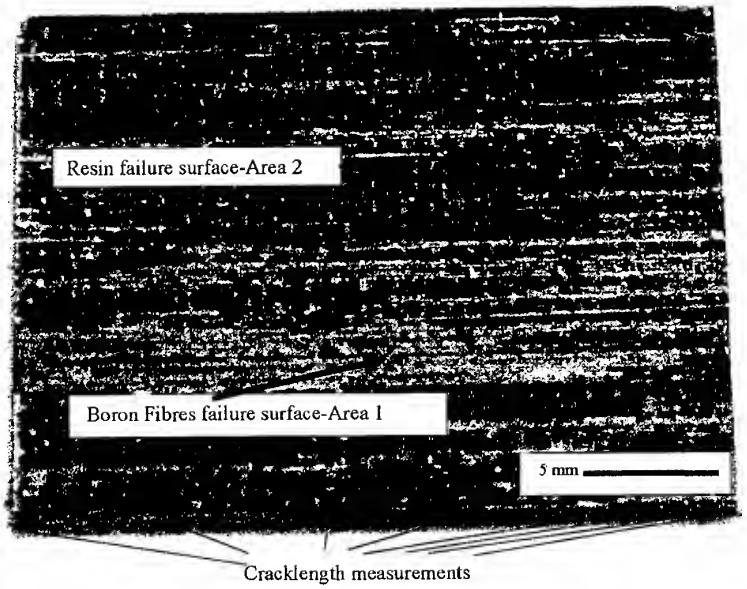

Figure 6.1 *Digital image of fracture surface of Standard 5521/4 laminate*

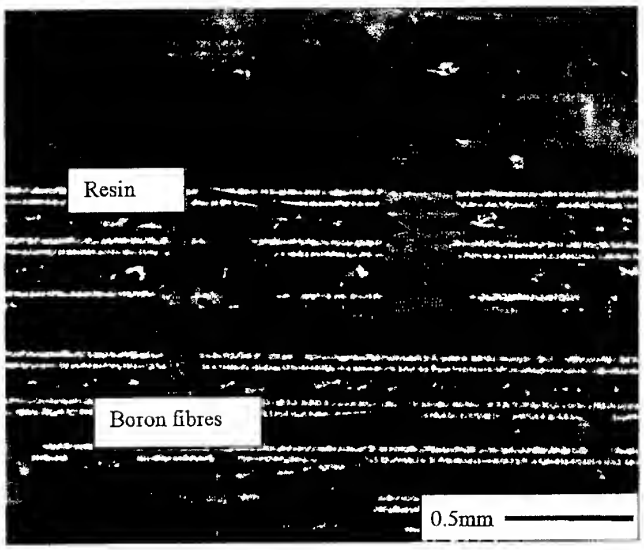

Figure 6.2 *Optical image of fracture surface of Standard 5521/4 laminate*

Figures 6.1 and 6.2 show that the standard 5521/4 laminate displays two types of fracture area. In one region failure appears to propagate through the laminate resin and in other regions evidence for interfacial failure between the fibre and resin exists.

6.2 Optical Analysis 5521/4 laminate co-cured with FM73

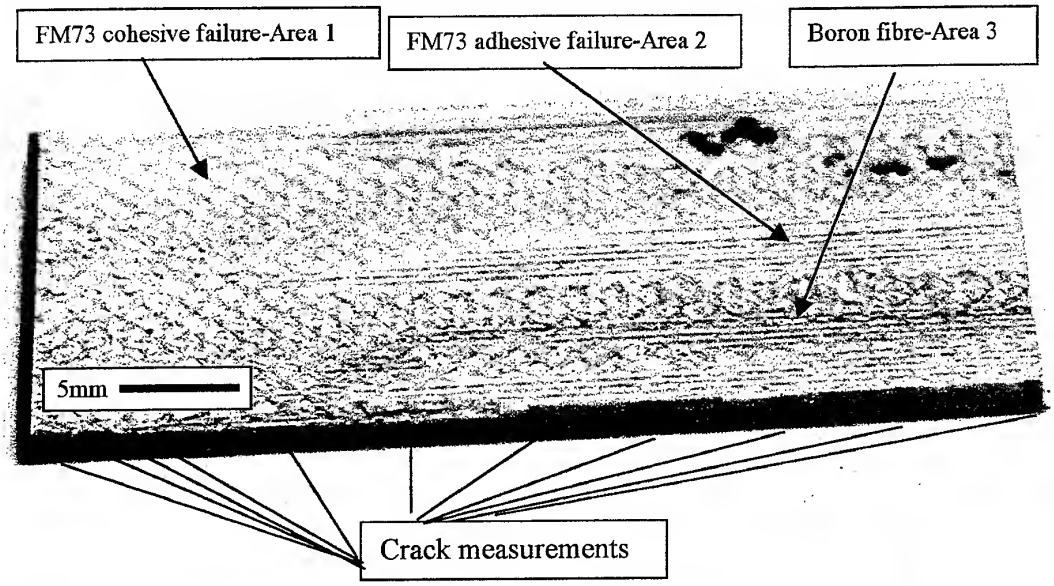

Figure 6.3 Digital image of fracture surface of 5521/4 laminate co-cured with FM73

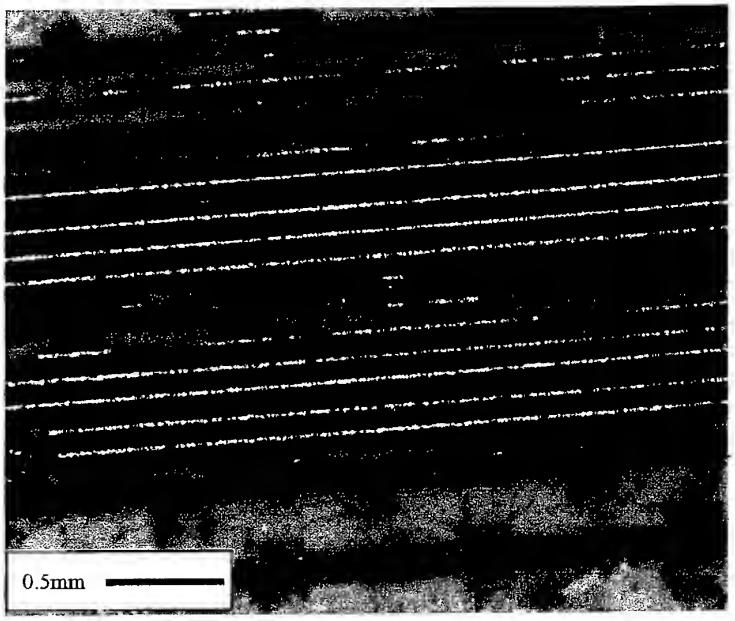

Figure 6.4 Optical image of fracture surface of 5521/4 laminate co-cured with FM73

Figures 6.3 and 6.4 show that there are two modes of failure occurring for the 5521/4 laminate co-cured with FM73. The two regions present indicate failure occurs either within the FM73 adhesive layer or at the fibre and FM73 adhesive interfacial region.

6.3 Optical Analysis of 5521/4 laminate co-cured with resin infused layers

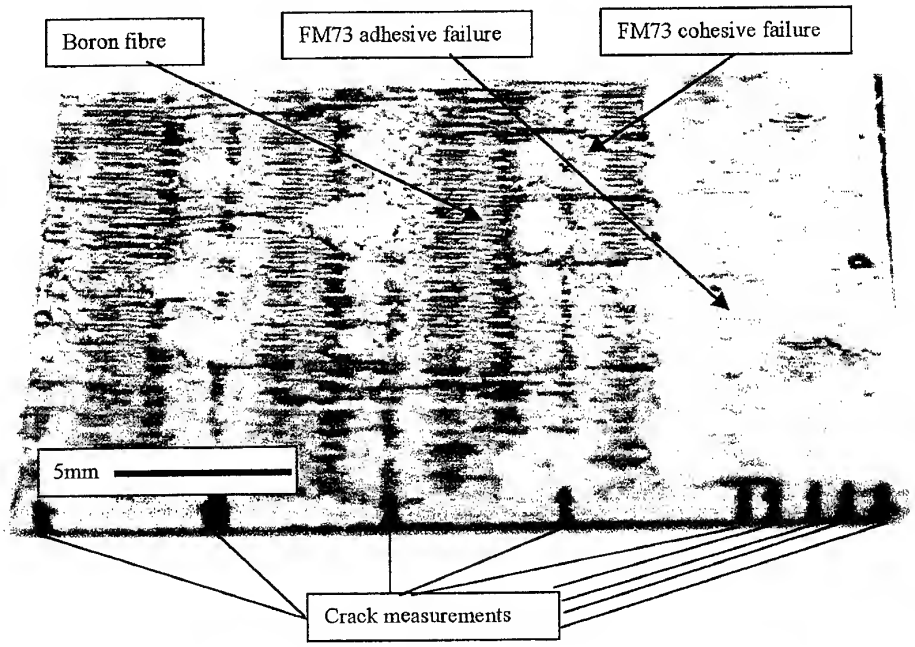

Figure 6.5 Digital image of 5521/4 laminate co-cured with resin infused layers

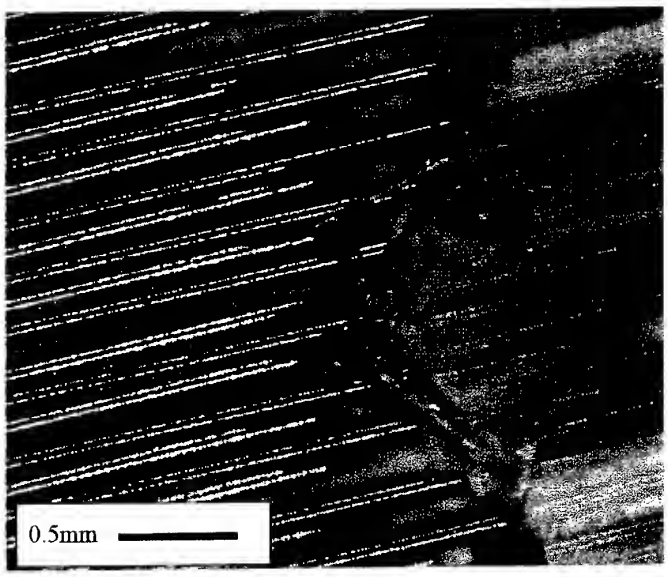

Figure 6.6 Optical image of 5521/4 laminate co-cured with resin infused layers

Figures 6.5 and 6.6 show that there are two modes of failure occurring for the 5521/4 laminate co-cured with the resin infused layers. The two regions present indicate failure occurs either within the FM73 adhesive layer or at the fibre and FM73 adhesive interfacial region. This is similar to the 5521/4 laminate co-cured with the FM73, however, Figure 6.5 shows that more failure appears to have propagated at the FM73-boron interface than in Figure 6.3.

6.4 SEM Analysis of Standard 5521/4 laminate

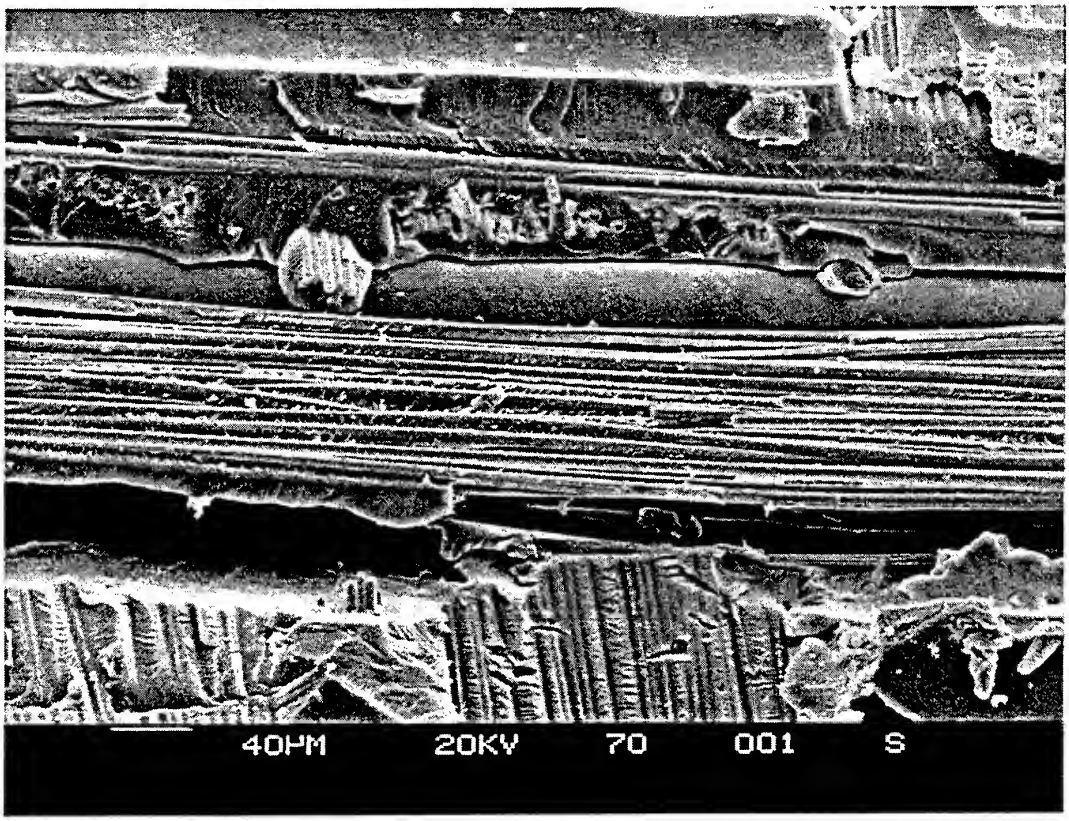

Figure 6.7 *SEM failure surface of Standard 5521/4 laminate, indicating cohesive resin and adhesive resin failure.*

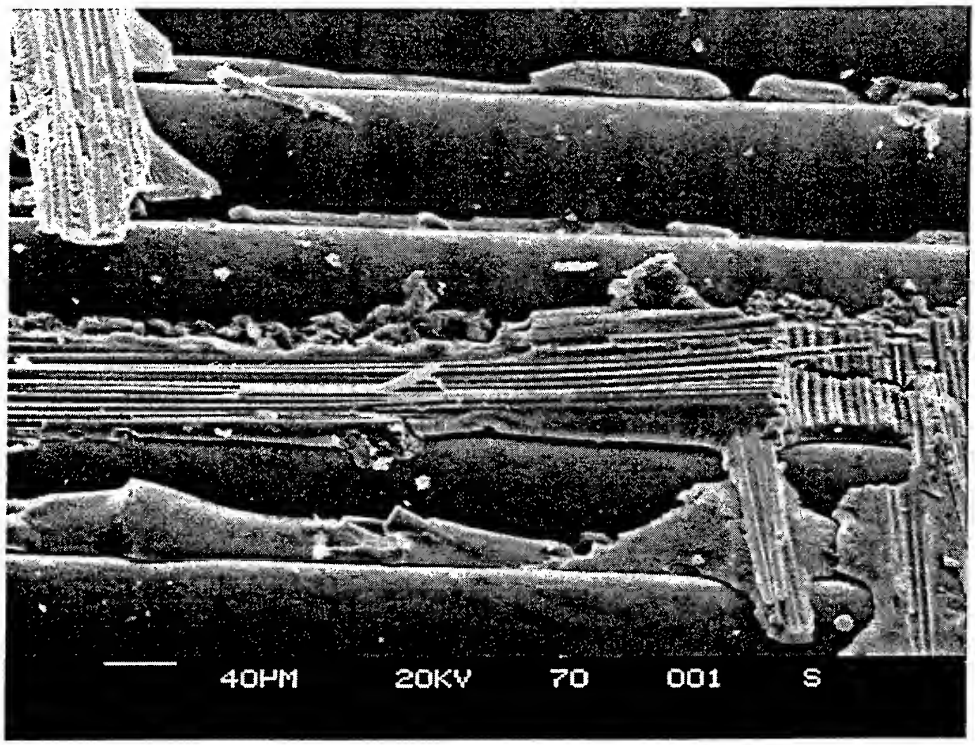

Figure 6.8 SEM failure surface of Standard 5521/4 laminate, indicating cohesive resin failure and the boron fibre adhesive failure surface.

Figures 6.7 and 6.8 indicate the complementary fracture surfaces from the standard 5521/4 laminate. Failure appears to occur either at the interface between the resin and fibre or within the resin layer itself.

6.5 SEM Analysis 5521/4 laminate co-cured with FM73

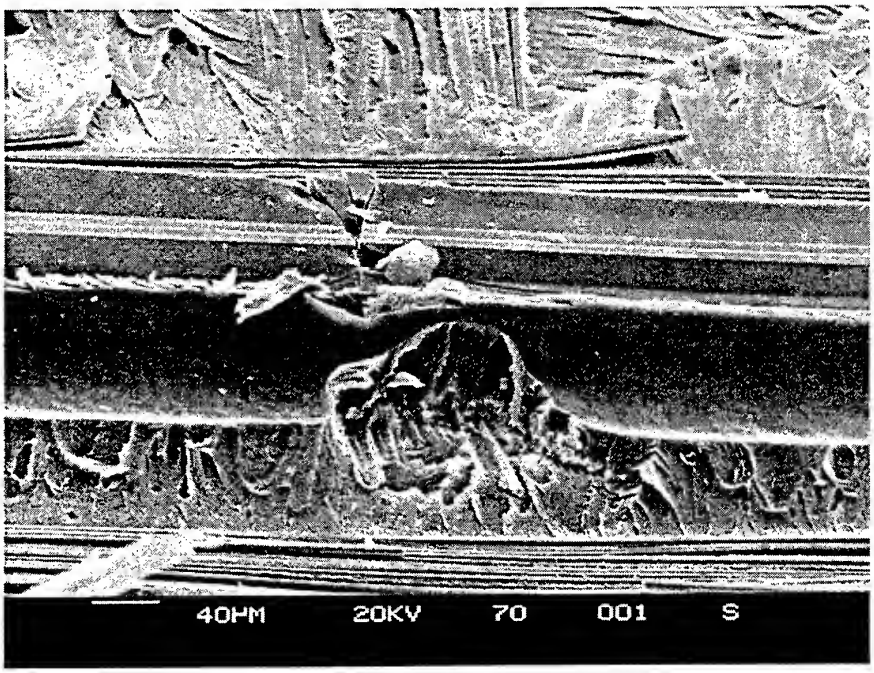

Figure 6.9 *Adhesive failure between fibre and resin and cohesive failure of resin for 5521/4 laminate co-cured with FM73.*

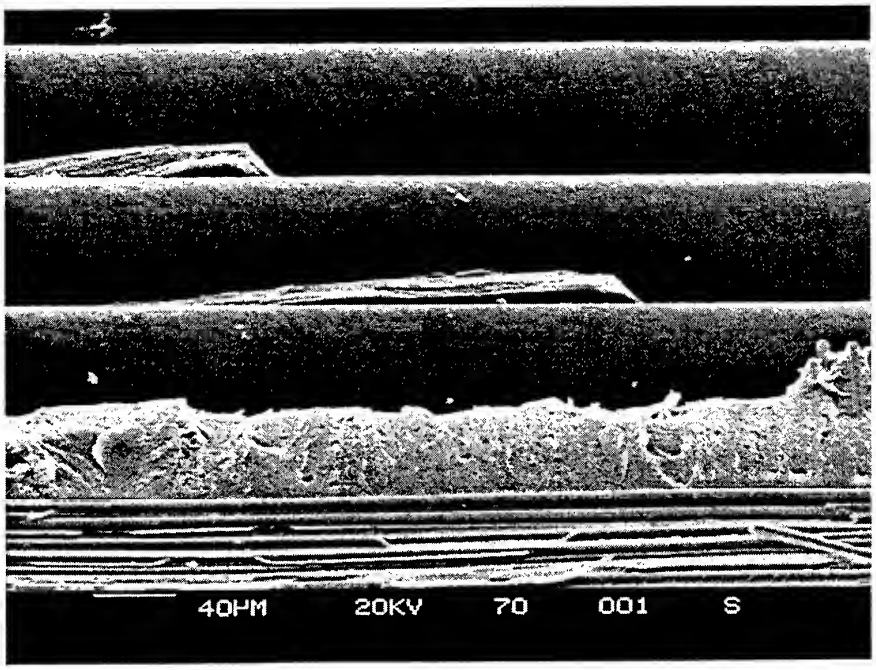

Figure 6.10 *Adhesive failure at the fibre surface for 5521/4 laminate co-cured with FM73*

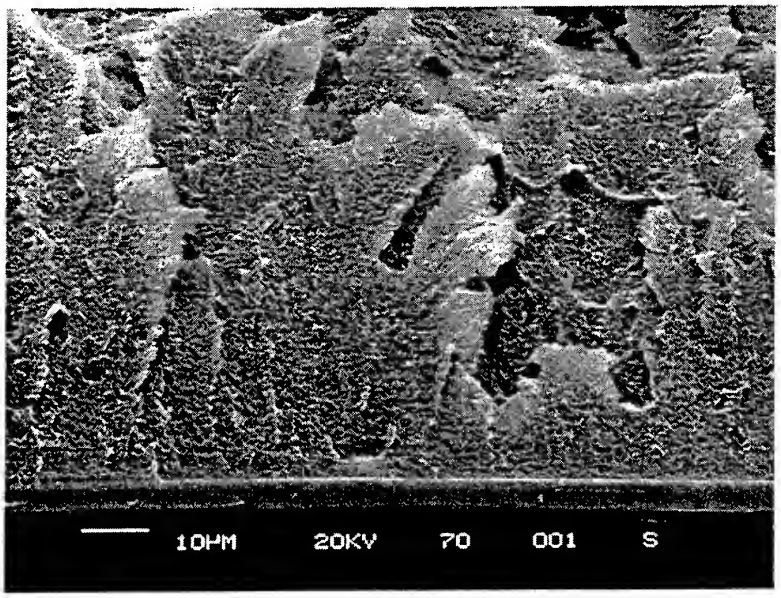

Figure 6.11 Cohesive failure of FM73 layer in 5521/4 laminate co-cured with FM73

Figures 6.9 to 6.11 indicate the different modes of failure observed for the 5521/4 laminate co-cured with FM73. In Figure 6.9 the failure appears to propagate at the resin-fibre interface as evidenced by the smooth fibre indentation. Cohesive fracture within the resin layer is also evident in the regions below and above the fibre indentation area. Figure 6.10 shows the fibre surfaces are free of adhesive, confirming the interfacial failure mode suggested in Figure 6.9. The voided adhesive region between two fibres also provides evidence that the FM73 layer has diffused between the fibres and failed cohesively in some regions. A higher magnification region of the cohesively failed FM73 layer observed in Figure 6.10 is shown in Figure 6.11. Voids and furrows on the adhesive fracture surface are typical of plastic deformation processes that occur in rubber toughened epoxy adhesives during fracture.

6.6 SEM Analysis 5521/4 laminate co-cured with resin infused layers

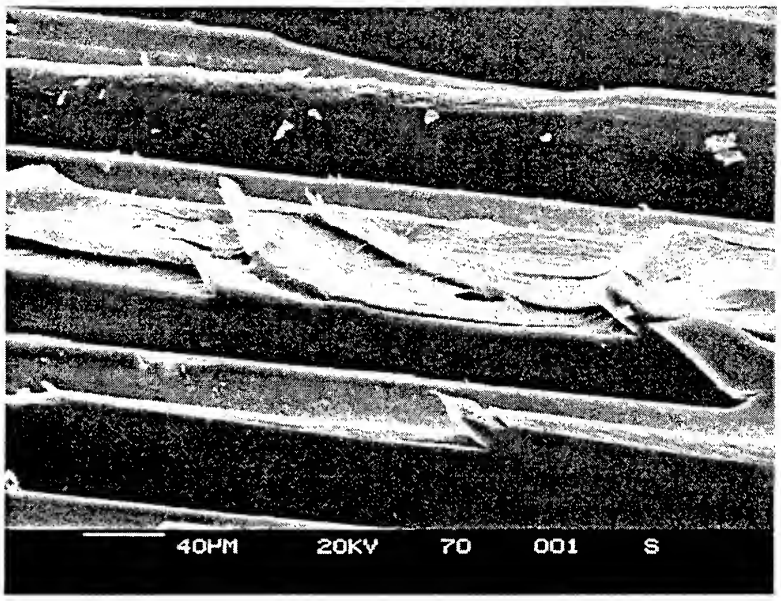

Figure 6.12 *Adhesive fracture of FM73 to boron interface for 5521/4 laminate co-cured with resin infused layers, FM73 surface.*

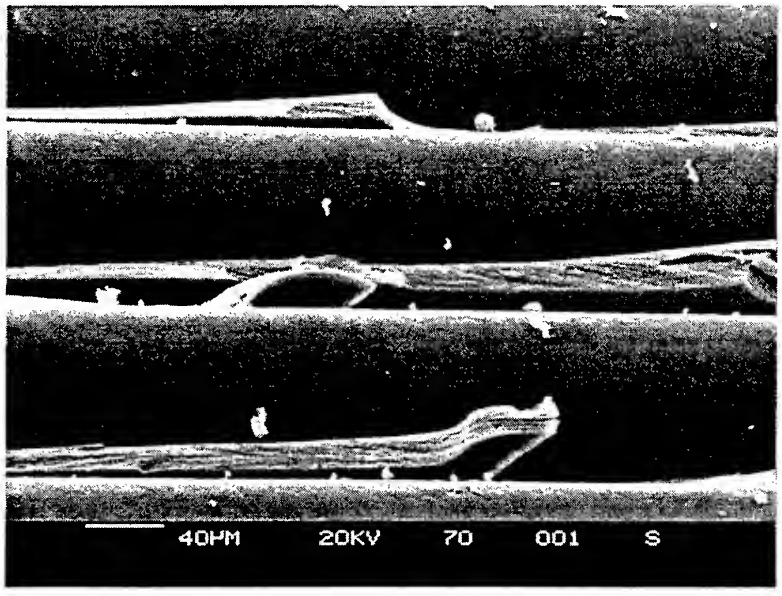

Figure 6.13 *Adhesive fracture of FM73 to boron interface for 5521/4 laminate co-cured with resin infused layers, boron fibre surface.*

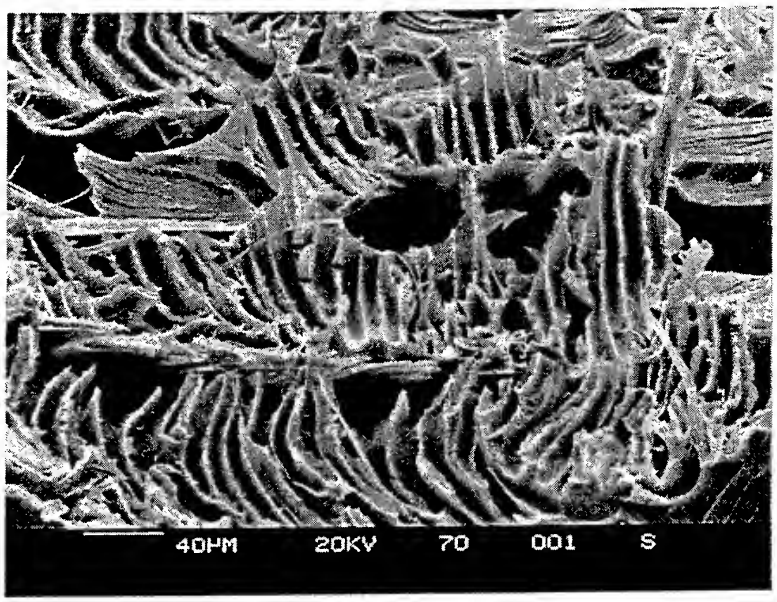

Figure 6.14 *Cohesive fracture of FM73 for 5521/4 laminate co-cured with resin infused layers, FM73 pulled between fibres.*

Figures 6.12 to 6.14 indicate the failure surfaces for the 5521/4 laminate co-cured with resin infused layers. Figure 6.12 shows the adhesive failure surface. There appears to be fracture at the boron fibre-FM73 interface and within the FM73 layer. Figure 6.13 shows the complementary fracture surface. The boron fiber surface shows no evidence of adhesive, confirming interfacial fracture has occurred between the fibre and FM73. Adhesive that has diffused between the fibers has failed cohesively in some regions also. A higher magnification image of the FM73 cohesive failure in Figure 14 shows that plastic deformation processes in the adhesive may be different to those observed in Figure 6.11 for the 5521/4 laminate co-cured with FM73.

6.7 XPS FractureAnalysis

Evidence provided by the SEM images in sections 6.4 to 6.6 of the interlaminar fracture processes suggested that interfacial failure of the resin or FM73 to boron fibre bond was a common fracture mode. XPS was employed to analyse the surfaces exposing boron fibres to establish that the failure mode was truly interfacial in these areas.

Table 6.1 Surface atomic composition of adhesive failure region of Standard 5521/4 laminate.

%B	%Si	%C	%N	%O	%Na
14.4	2.5	53.1	5.7	21.9	2.5

Table 6.2 Surface atomic composition of adhesive failure region of 5521/4 laminate co-cured with FM73.

%B	%Si	%C	%N	%O	%Na
15.5	1.4	57.3	1.9	22.0	2.0

Table 6.3 Surface atomic composition of adhesive failure region of 5521/4 laminate co-cured with resin infused layers.

%B	%Si	%C	%N	%O	%Na
14.9	17.6	41.9	0.4	24.6	0.6

The boron fracture surfaces all indicate signficant levels of boron which suggests that fracture occurs in close proximity to the boron and resin interface. The presence of carbon, silicon and oxygen may suggest the presence of some resin in the fracture region also. Based on the images shown in sections 6.4 to 6.6 the surface signal may have a contribution from the adhesive that has failed between adjacent fibres, refer Figures 6.8, 6.10 and 6.13. Characterisation of the boron fibre surface is also required to verify the fracture path. This is undertaken in section 7.

7. Surface Characterisation of Boron Fibres

XPS analysis of the as received boron fibres was performed in order to characterise the boron fibre surface chemistry. Table 7.1 indicates the surface composition and binding energy position of the boron fibres.

Table 7.1 XPS analysis of as received boron fibre surface.

	B	Si	C	O
Atomic Conc.(%)	22.6	15.8	38.1	23.5
Binding energy(eV)	187.2	101.8	285.0	532.3

Figure 7.1 indicates the concentration of the elements in Table 7.1 as a function of depth. This data was acquired using ion milling of the boron fibre surface in conjunction with XPS analysis. The time scale represents an approximate etch rate of 2nm/minute. The XPS data shows that the boron fibre is covered with a thin silicon containing organic layer which may be less than 10nm. The binding energy positions of the elements present on the surface of the fibre are consistent with an organic material.

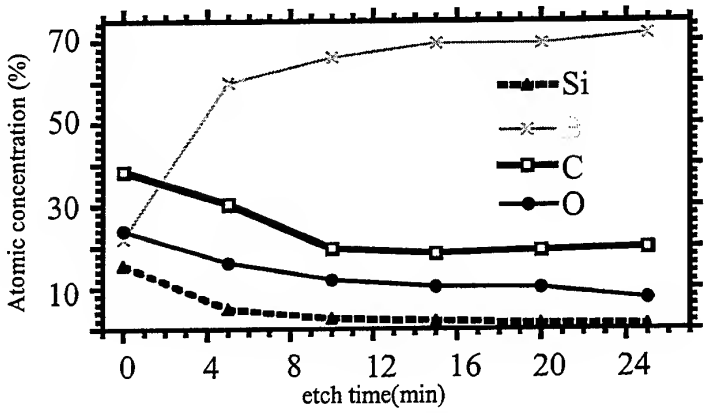

Figure 7.1 *Depth profile of a 100μm boron fibre. Etch rate is approximately equal to 2nm/min.*

8. Discussion

The data shown in Table 5.1 essentially indicates that incorporation of FM73 into the laminate layers in the zone of fracture can increase the fracture toughness from a value of approximately 330J/m² to around 2000J/m². This is approaching a fracture toughness value which is found for FM73 adhesive [3]. Whilst the process of co-curing FM73 with the 5521/4 laminate provided the highest initiation fracture toughness, this fracture appeared to be unstable, as shown in Figure 5.4. The process of co-curing FM73 film infused boron layers produced a more stable fracture. Both the co-cured and film infused specimens, refer Figures 3.2 and 3.3, however, exhibited more complex fracture modes than the standard boron/epoxy laminate.

Some insight into the modes of fracture and the processes limiting the fracture toughness of the laminates may be developed from fracture observations shown in section 6.

The standard 5521/4 laminate exhibits a mixed mode of fracture between the fibre and resin interface and within the resin itself. Figures 6.1 and 6.2 provide an example of the typical failure surfaces observed and the relative areas of the two types of failure. SEM analysis shows higher magnification images of the two types of failure in Figures 6.7 and 6.8. XPS analysis of the failure surface of the standard 5521/4 laminate shows boron, silicon and carbon, suggesting that the failure between the resin and fibre is truly interfacial. The presence of silicon is an indication of the organic layer observed on the boron surface in section 7, refer Table 7.1 and Figure 7.1.

The 5521/4 laminate co-cured with FM73 also exhibits three modes of failure as indicated in Figures 6.3 and 6.4. Failure occurs both within the FM73 layer, interfacially between the resin and boron fibre and cohesively within the resin. Higher magnification images of these failure modes are provided by SEM images in Figures 6.9, 6.10 and 6.11. The XPS fracture analysis in the adhesive failure regions, shown in Table 6.2, shows a similar composition to that observed for the 5521/4 laminate, refer Table 6.1, and support for the interfacial failure mode between fibre and resin. The high G_I values observed for the initial cracklengths, shown in Figure 5.2, can be seen to correspond to the cohesive failure within the FM73 layer, refer Figure 6.3. The lower G_1 values at larger cracklengths correspond to an increase in the adhesive failure mode between the fibre and the resin and the cohesive failure in the resin ie. some fracture has moved from the FM73 layer to the 5521/4 laminate layer, where fracture typical of that layer influences the fracture toughness value.

The 5521/4 laminate co-cured with resin infused layers exhibits two modes of failure as indicated in Figures 6.5 and 6.6. Failure occurs both within the FM73 layer and interfacially between the FM73 and boron fibre. Higher magnification images of these failure modes are provided by SEM images in Figures 6.12, 6.13 and 6.14. XPS analysis of the adhesive failure surface, refer Table 6.3, shows a higher level of silicon than for the two previous failure surfaces and may be indicative of an increase in the mode of failure between the organic layer present on the boron fibre and the FM73 layer. The more consistent fracture toughness observed for the 5521/4 laminate co-cured with resin infused layers, relative to the 5521/4 laminate co-cured with FM73, appears to be related to the consistent nature of the fracture path observed in the former. The failure appears to be predominantly interfacial between the fibre and FM73 layer, although some regions where diffused FM73 has failed cohesively were observed, refer Figure 6.14.

9. Conclusion

Improvement of the fracture toughness of the 5521/4 laminate can be achieved by the incorporation of rubber toughened FM73 layers in the fracture plane. Whilst the 5521/4 laminate co-cured with FM73 exhibited a high initial fracture toughness value, fracture was unstable as a result of some fracture propagation into the brittle 5521/4 laminate layer. Stable fracture was achieved for a 5521/4 laminate co-cured with FM73 infused layers. The initial fracture toughness was not as high as the 5521/4 laminate co-cured with FM73 as interfacial failure between the fibre and rubber toughened epoxy layer was observed as the primary failure mode. The initial toughness of the film infused laminate was, however, 500% higher than for the standard laminate

The process used to fabricate the 5521/4 laminate co-cured with FM73 infused layers could be used in certain aircraft repairs where it is known that very high stresses may

be experienced during service. In these cases the the low energy fracture of the standard boron/epoxy laminate could be expected.

Further studies may look at improved methods to increase the fracture toughness of the laminate layers by developing procedures to incorporate rubber toughened epoxy resin in the zones of higher stress. Alternatively, as suggested by the interfacial failure mode observed for the 5521/4 laminate co-cured with FM73 infused layers, improved interfacial adhesion may also provide a means of improving the laminate fracture toughness.

10. References

1. Chalkley, P. D. and Geddes, R., "Fatigue Testing of Bonded Joints Representative of the F-111C WPF Upper Plate Doublers", DSTO Research Report 1999.
2. ASTM, Annual Book of Standards, Section 15, vol 15.03, Space Simulation. Philadelphia: ASTM, 1998-ASTM D5528, "Mode I Interlaminar Fracture Toughness of Unidirectional Fiber-Reinforced Polymer Matrix Composites".
3. Chalkley, P. D., "A Critical Compendium of Material Property Data for Bonded-Composite Repairs", Divisional Discussion Paper, DSTO-DDP-0274

Appendix A:

Table 1 has the specimen dimensions for the six specimens in the three series of specimens.

Table 1. Specimen dimensions –average of three measurements .

	b (mm)						h (mm)					
	1	2	3	4	5	6	1	2	3	4	5	6
16 plies 5521/4	19.88	-	19.86	19.87	19.83	-	2.19	-	2.20	2.19	2.20	-
16 plies 5521/4 co-cured with 2 layers FM73	19.84	19.90	19.88	19.89	19.87	19.96	2.85	2.98	2.99	2.99	2.97	2.88
14 plies 5521/4, 2 plies of FM73 infused boron fibres	19.94	20.05	20.02	20.16	20.07	19.75	2.74	2.75	2.76	2.74	2.80	2.72

The specimens made from sixteen plies of 5521/4 and co-cured with two layers of FM73 did not meet the ASTM requirements for uniformity of thickness (variation in measure "b" shall not exceed 0.1 mm). Typical measurements made at one end, the middle and the other end were: 3.00 mm, 3.27 mm and 2.69 mm. This non-uniformity could be avoided through the use of a stiff plate on top of the laminate during cure in the autoclave.

Results for each specimen are presented in the following tables.

5521/4 specimens

Specimen 1 test results.

Crack length nom.	Crack length actual (mm)	P (N)	δ (mm)	G_{mbt} (J/m²)	G_{cc} (J/m²)
a0	50.86	34.0	7.9	386	384
a1	51.71	37.0	8.5	445	442
a2	52.69	39.0	9.2	498	495
a3	53.96	39.5	10.0	536	532
a4	54.90	39.2	10.2	533	529
a5	55.88	39.0	10.6	542	538
a10	60.68	40.0	13.6	658	652
a15	65.82	36.0	16.4	660	652
a20	70.96	31.5	18.0	589	581
a25	75.80	28.0	19.6	535	526

Note: mbt stands for modified beam theory and cc stands for compliance calibration (see ASTM)

Specimen 3 test results.

Crack length nom.	Crack length actual (mm)	P (N)	δ (mm)	G_{mbt} (J/m²)	G_{cc} (J/m²)
a0	50.70	28.0	7.9	272	283
a1	51.60	28.0	7.9	268	278
a2	52.83	29.2	8.6	298	308
a3	53.64	29.8	9.2	322	332
a4	54.64	29.5	9.8	334	343
a5	55.81	29.0	10.4	342	351
a10	60.64	27.2	12.1	348	352
a15	65.80	26.0	14.4	369	369
a20	70.66	25.5	17.7	419	414
a25	75.78	28.5	20.3	505	495

Specimen 4 test results.

Crack length nom.	Crack length actual (mm)	P (N)	δ (mm)	G_{mbt} (J/m²)	G_{cc} (J/m²)
a0	48.48	31.0	7.8	340	346
a1	49.70	32.0	8.4	370	375
a2	50.70	32.0	8.8	381	385
a3	51.75	31.5	9.2	384	388
a4	52.48	31.2	9.5	388	391
a5	53.54	31.0	9.8	391	393
a10	58.69	29.0	11.8	405	404
a15	63.64	28.0	14.5	445	442
a20	68.68	26.2	17.2	461	455
a25	73.71	25.2	19.4	468	460

Specimen 5 test results.

Crack length nom.	Crack length actual (mm)	P (N)	δ (mm)	G_{mbt} (J/m²)	G_{cc} (J/m²)
a0	49.87	28.5	8.2	313	319
a1	50.87	30.0	8.8	347	353
a2	52.01	30.2	9.6	374	379
a3	53.00	30.2	9.6	367	372
a4	53.90	30.0	10.6	397	401
a5	55.06	29.5	11.0	398	401
a10	59.98	27.5	12.6	393	393
a15	64.91	25.2	14.2	378	375
a20	69.95	23.5	16.6	385	379
a25	74.82	21.5	18.2	363	356

16 plies 5521/4 co-cured with FM73 specimens

Specimen 1 test results.

Crack length nom.	Crack length actual (mm)	P (N)	δ (mm)	G_{mbt} (J/m²)	G_{cc} (J/m²)
a0	50.25	127.0	25.6	2390	2528
a1	51.05	139.0	27.8	2819	2957
a2	52.19	150.0	32.0	3464	3593
a3	53.17	155.0	33.8	3746	3850
a4	54.15	158.0	36.6	4097	4172
a5	55.02	157.0	37.4	4126	4170
a10	60.28	148.0	39.8	3946	3818
a15	65.23	148.0	39.8	3780	3528
a20	70.21	148.0	39.8	3627	3278
a25	75.16	98.0	45.6	2645	2323

Note: mbt stands for modified beam theory and cc stands for compliance calibration (see ASTM)

Specimen 2 test results.

Crack length nom.	Crack length actual (mm)	P (N)	δ (mm)	G_{mbt} (J/m²)	G_{cc} (J/m²)
a0	49.35	126.0	22.4	3784	3821
a1	50.29	151.0	27.6	5496	5538
a2	50.35	155.0	28.4	5799	5842
a3	52.27	159.0	29.8	6039	6058
a4	53.09	160.0	30.8	6195	6203
a5	54.25	160.0	30.8	6077	6070
a10	59.36	123.0	33.4	4675	4624
a15	64.23	108.0	35.4	4053	3977
a20	69.06	98.0	40.2	3911	3812
a25	74.20	90.0	46.0	3849	3728

Specimen 3 test results.

Crack length nom.	Crack length actual (mm)	P (N)	δ (mm)	G_{mbt} (J/m²)	G_{cc} (J/m²)
a0	48.92	91.0	15.8	2163	2356
a1	50.03	120.0	21.0	3709	4038
a2	51.11	153.0	27.0	5956	6480
a3	52.15	162.0	29.6	6778	7371
a4	53.26	161.0	31.2	6956	7561
a5	54.27	60.0	31.6	2578	2801
a10	59.40	60.0	31.6	2360	2559
a15	64.00	60.0	31.6	2193	2375
a20	69.31	60.0	31.6	2028	2193
a25	74.10	60.0	31.6	1899	2051

Specimen 4 test results.

Crack length nom.	Crack length actual (mm)	P (N)	δ (mm)	G_{mbt} (J/m²)	G_{cc} (J/m²)
a0	50.25	117.0	21.4	3392	4300
a1	51.21	126.0	23.2	3893	4926
a2	52.36	158.0	30.0	6187	7812
a3	53.35	160.0	31.2	6406	8074
a4	54.35	157.0	32.4	6419	8077
a5	55.21	155.0	32.8	6324	7946
a10	60.19	60.0	33.0	2276	2839
a15	65.71	60.0	33.0	2099	2600
a20	70.61	60.0	33.0	1964	2420
a25	75.42	60.0	33.0	1847	2265

Specimen 5 test results.

Crack length nom.	Crack length actual (mm)	P (N)	δ (mm)	G_{mbt} (J/m²)	G_{cc} (J/m²)
a0	50.36	120.0	22.0	3629	1841
a1	51.29	157.0	30.0	6366	3225
a2	52.28	160.0	31.0	6588	3332
a3	53.20	163.0	32.4	6902	3486
a4	54.11	0.0	32.4	0	0
a5	55.26	0.0	32.4	0	0
a10	60.23	0.0	32.4	0	0
a15	65.27	0.0	32.4	0	0
a20	70.44	0.0	32.4	0	0
a25	75.37	0.0	32.4	0	0

Specimen 6 test results.

Crack length nom.	Crack length actual (mm)	P (N)	δ (mm)	G_{mbt} (J/m²)	G_{cc} (J/m²)
a0	49.49	114.0	21.0	3296	3331
a1	50.29	134.0	25.2	4582	4624
a2	51.48	150.0	30.8	6137	6180
a3	52.49	150.0	32.0	6264	6297
a4	53.46	151.0	34.0	6589	6612
a5	54.48	151.0	35.2	6705	6718
a10	59.34	144.0	41.6	6987	6952
a15	64.50	128.0	45.4	6275	6204
a20	69.58	106.0	51.2	5462	5371
a25	74.37	96.0	53.8	4885	4782

14 plies 5521/4 co-cured with 2 plies of film-infused boron

Specimen 1 test results.

Crack length nom.	Crack length actual (mm)	P (N)	δ (mm)	G_{mbt} (J/m²)	G_{cc} (J/m²)
a0	49.41	71.0	15.0	1380	1442
a1	50.51	91.0	19.6	2268	2363
a2	51.60	110.0	26.0	3570	3708
a3	52.53	109.0	26.6	3565	3693
a4	53.48	110.0	26.8	3569	3688
a5	52.72	103.0	28.6	3610	3738
a10	59.66	108.0	37.4	4447	4530
a15	64.70	70.0	37.6	2699	2722
a20	69.54	70.0	37.6	2532	2532
a25	74.52	85.0	47.4	3644	3617

Note: mbt stands for modified beam theory and cc stands for compliance calibration (see ASTM)

Specimen 2 test results.

Crack length nom.	Crack length actual (mm)	P (N)	δ (mm)	G_{mbt} (J/m²)	G_{cc} (J/m²)
a0	50.98	89.0	20.6	2028	2099
a1	51.90	101.0	23.4	2579	2657
a2	52.91	110.0	26.4	3123	3203
a3	53.87	113.5	28.6	3443	3516
a4	55.00	115.0	29.8	3578	3636
a5	55.85	115.0	29.8	3536	3581
a10	60.98	113.0	29.8	3245	3222
a15	65.93	92.0	40.4	3367	3290
a20	70.84	88.0	46.0	3461	3335
a25	75.97	94.0	49.8	3781	3596

Specimen 3 test results.

Crack length nom.	Crack length actual (mm)	P (N)	δ (mm)	G_{mbt} (J/m²)	G_{cc} (J/m²)
a0	50.87	80.0	16.4	1537	1533
a1	51.91	88.0	20.4	2070	2056
a2	52.88	92.0	21.8	2278	2255
a3	53.79	92.0	21.8	2247	2216
a4	54.82	92.0	21.8	2213	2175
a5	55.86	114.0	30.0	3717	3640
a10	60.82	115.0	36.4	4245	4092
a15	66.03	162.0	42.4	6506	6184
a20	70.89	104.0	51.0	4733	4448
a25	75.80	88.0	55.2	4095	3809

Specimen 4 test results.

Crack length nom.	Crack length actual (mm)	P (N)	δ (mm)	G_{mbt} (J/m²)	G_{cc} (J/m²)
a0	49.62	78.0	17.3	1795	1807
a1	50.53	93.0	21.0	2557	2568
a2	51.44	97.0	22.1	2762	2769
a3	52.46	116.0	27.2	3994	3996
a4	53.38	118.0	29.0	4266	4259
a5	54.45	118.0	29.0	4190	4175
a10	59.42	109.5	33.2	4115	4065
a15	64.51	80.0	38.9	3270	3205
a20	69.39	87.0	42.6	3643	3549
a25	-	-	-	-	-

Specimen 5 test results.

Crack length nom.	Crack length actual (mm)	P (N)	δ (mm)	G_{mbt} (J/m²)	G_{cc} (J/m²)
a0	49.84	63.0	14.0	1218	1245
a1	50.74	72.0	16.4	1604	1637
a2	51.87	103.0	25.8	3537	3604
a3	52.88	106.0	27.4	3797	3864
a4	53.71	100.0	27.6	3557	3615
a5	54.73	100.0	27.6	3495	3548
a10	59.82	88.0	34.4	3529	3560
a15	64.72	82.0	40.2	3570	3583
a20	69.79	84.0	47.6	4034	4031
a25	74.78	81.0	54.2	4150	4130

Specimen 6 test results.

Crack length nom.	Crack length actual (mm)	P (N)	δ (mm)	G_{mbt} (J/m²)	G_{cc} (J/m²)
a0	50.36	120.0	22.0	1840	1827
a1	51.29	157.0	30.0	2437	2415
a2	52.28	160.0	31.0	2568	2541
a3	53.20	163.0	32.4	3133	3094
a4	54.11	0.0	32.4	3082	3039
a5	55.26	0.0	32.4	3033	2987
a10	60.23	0.0	32.4	3377	3302
a15	65.27	0.0	32.4	3209	3121
a20	70.44	0.0	32.4	4180	4044
a25	75.37	0.0	32.4	4187	4034

DISTRIBUTION LIST

Development of Film-Infused Tougher Boron/Epoxy Ply

Peter Chalkley, Ivan Stoyanovski, Richard Muscat and Andrew Rider

AUSTRALIA

DEFENCE ORGANISATION

Task Sponsor
ASI4A
DGTA

S&T Program
Chief Defence Scientist
FAS Science Policy } shared copy
AS Science Corporate Management
Counsellor Defence Science, London (Doc Data Sheet)
Counsellor Defence Science, Washington (Doc Data Sheet)
Scientific Adviser to MRDC Thailand (Doc Data Sheet)
Scientific Adviser Policy and Command
Navy Scientific Adviser (Doc Data Sheet and distribution list only)
Scientific Adviser - Army (Doc Data Sheet and distribution list only)
Air Force Scientific Adviser (Doc Data Sheet and distribution list only)
Director Trials

Aeronautical and Maritime Research Laboratory
Director
Chief of Airframes and Engines. Division
Alan Baker
Richard Chester
Peter Chalkley
Andrew Rider
Roger Vodicka
Ivan Stoyanovski

DSTO Library and Archives
Library Fishermans Bend (Doc Data sheet)
Library Maribyrnong(Doc Data sheet)
Library Salisbury
Australian Archives
Library, MOD, Pyrmont (Doc Data sheet)
US Defense Technical Information Center, 2 copies
UK Defence Research Information Centre, 2 copies
Canada Defence Scientific Information Service, 1 copy

NZ Defence Information Centre, 1 copy
National Library of Australia, 1 copy

Capability Systems Staff
Director General Maritime Development (Doc Data sheet)
Director General C31 Development (Doc Data sheet)
Director General Aerospace Development (Doc Data sheet)

Army
ASNSO ABCA, Puckapunyal, (4 copies)
SO(Science), DJFHQ(L), MILPO Enoggera, Queensland 4051 (Doc Data Sheet only)

Air Force
ASI-SRS

Intelligence Program
DGSTA Defence Intelligence Organisation
Manager, Information Centre, Defence Intelligence Organisation

Corporate Support Program
Library Manager, DLS-Canberra (Doc Data sheet)

UNIVERSITIES AND COLLEGES
Australian Defence Force Academy
Library
Head of Aerospace and Mechanical Engineering
Serials Section (M list), Deakin University Library, Geelong 3217
Hargrave Library, Monash University (Doc Data sheet)
Librarian, Flinders University

OTHER ORGANISATIONS
NASA (Canberra)
AusInfo

OUTSIDE AUSTRALIA

ABSTRACTING AND INFORMATION ORGANISATIONS
Library, Chemical Abstracts Reference Service (Doc Data sheet only)
Engineering Societies Library, US (Doc Data sheet only)
Materials Information, Cambridge Scientific Abstracts, US (Doc Data sheet only)
Documents Librarian, The Center for Research Libraries, US (Doc Data sheet only)

INFORMATION EXCHANGE AGREEMENT PARTNERS
Acquisitions Unit, Science Reference and Information Service, UK (Doc Data sheet only)

Library - Exchange Desk, National Institute of Standards and Technology, US (Doc Data sheet only)
National Aerospace Laboratory, Japan (Doc Data sheet only)
National Aerospace Laboratory, Netherlands (Doc Data sheet only)

SPARES (5 copies)

Total number of copies: 39

DEFENCE SCIENCE AND TECHNOLOGY ORGANISATION DOCUMENT CONTROL DATA

1. PRIVACY MARKING/CAVEAT (OF DOCUMENT)

2. TITLE

Development of Film-Infused Tougher Boron/Epoxy Ply

3. SECURITY CLASSIFICATION (FOR UNCLASSIFIED REPORTS THAT ARE LIMITED RELEASE USE (L) NEXT TO DOCUMENT CLASSIFICATION)

Document (U)
Title (U)
Abstract (U)

4. AUTHOR(S)

Peter Chalkley, Ivan Stoyanovski, Richard Muscat and Andrew Rider

5. CORPORATE AUTHOR

Aeronautical and Maritime Research Laboratory
PO Box 4331
Melbourne Vic 3001 Australia

6a. DSTO NUMBER	6b. AR NUMBER	6c. TYPE OF REPORT	7. DOCUMENT DATE
DSTO-TN-0308	AR-011-599	Technical Note	October 2000

8. FILE NUMBER	9. TASK NUMBER	10. TASK SPONSOR	11. NO. OF PAGES	12. NO. OF REFERENCES
M1/8/1310	98/172	AIR	34	3

13. URL ON THE WORLD WIDE WEB

http://www.dsto.defence.gov.au/corporate/reports/DSTO-TN-0308.pdf

14. RELEASE AUTHORITY

Chief, Airframes and Engines Division

15. SECONDARY RELEASE STATEMENT OF THIS DOCUMENT

Approved for Public Release

OVERSEAS ENQUIRIES OUTSIDE STATED LIMITATIONS SHOULD BE REFERRED THROUGH DOCUMENT EXCHANGE, PO BOX 1500, SALISBURY, SA 5108

16. DELIBERATE ANNOUNCEMENT

No Limitations

17. CASUAL ANNOUNCEMENT Yes

18. DEFTEST DESCRIPTORS

Aircraft repair, Aircraft maintenance, Bonded Repairs, Boron/Epoxy laminates

19. ABSTRACT

A previous study has examined the fatigue properties of bonded joints representative of the boron-epoxy doublers bonded to the wing-pivot fittings of Royal Australian Air Force (RAAF) F-111C aircraft. These repairs indicated some fatigue damage and crack propagation occurred at the boron fiber to adhesive interface of the doubler. This paper reports studies that have investigated methods to improve the fracture toughness of the boron/epoxy laminate. Two types of specimen were prepared. In the first case the standard boron epoxy laminate was modified by co-curing FM73 adhesive film layers at the midplane. In the second case a standard laminate with two FM73 film infused layers at the midplane was prepared. The two modified laminates showed substantial increases in the fracture toughness, however, the co-cured FM73 laminate did not exhibit stable fracture. Failure analysis indicated that the three laminate specimens tested exhibited a complex fracture. Fracture either propagated at the boron-epoxy interface or within the resin or FM73 layers. Further improvement in fracture toughness of the laminate may be achieved by improving the boron to FM73 adhesion. The methods reported for improving laminate fracture toughness may potentially be employed for aircraft repairs in which very high stresses are known to be present.